

Measurement of $\sigma(e^+e^- \rightarrow \pi^+\pi^-\gamma)$ and extraction of $\sigma(e^+e^- \rightarrow \pi^+\pi^-)$ below 1 GeV with the KLOE detector

The KLOE Collaboration

A. Aloisio^g, F. Ambrosino^g, A. Antonelli^c, M. Antonelli^c,
C. Bacci^m, M. Barva^m, G. Bencivenni^c, S. Bertolucci^c,
C. Bini^k, C. Bloise^c, V. Bocci^k, F. Bossi^c, P. Branchini^m,
S. A. Bulychjov^f, R. Caloi^k, P. Campana^c, G. Capon^c,
T. Capussela^g, G. Carboni^l, F. Ceradini^m, F. Cervelliⁱ,
F. Cevenini^g, G. Chiefari^g, P. Ciambrone^c, S. Conetti^o,
E. De Lucia^k, A. De Santis^k, P. De Simone^c, G. De Zorzi^k,
S. Dell’Agnello^c, A. Denig^{d 1}, A. Di Domenico^k,
C. Di Donato^g, S. Di Falcoⁱ, B. Di Micco^m, A. Doria^g,
M. Dreucci^c, O. Erriquez^a, A. Farilla^m, G. Felici^c, A. Ferrari^m,
M. L. Ferrer^c, G. Finocchiaro^c, C. Forti^c, P. Franzini^k,
C. Gatti^k, P. Gauzzi^k, S. Giovannella^c, E. Gorini^e,
E. Graziani^m, M. Incagliⁱ, W. Kluge^d, V. Kulikov^f,
F. Lacava^k, G. Lanfranchi^c, J. Lee-Franzini^{c,n}, D. Leone^d,
M. Martemianov^c, M. Martini^c, M. Matsyuk^c, W. Mei^c,
L. Merola^g, R. Messi^l, S. Miscetti^c, M. Moulson^c, S. Müller^d,
F. Murtas^c, M. Napolitano^g, F. Nguyen^m, M. Palutan^c,
E. Pasqualucci^k, L. Passalacqua^c, A. Passeri^m, V. Patera^{c,j},
F. Perfetto^g, E. Petrolo^k, L. Pontecorvo^k, M. Primavera^e,
P. Santangelo^c, E. Santovetti^l, G. Saracino^g,
R. D. Schambergerⁿ, B. Sciascia^c, A. Sciubba^{c,j}, F. Scuriⁱ,
I. Sfiligoi^c, A. Sibidanov^{c,h}, T. Spadaro^c, E. Spiriti^m,
M. Testa^k, L. Tortora^m, P. Valente^c, B. Valeriani^d,
G. Venanzoni^{c 2}, S. Veneziano^k, A. Ventura^e, S. Ventura^k,
R. Versaci^m, I. Villella^g, G. Xu^{c,b}

¹ Corresponding author: A. Denig, e-mail: Achim.Denig@iekp.fzk.de

² Corresponding author: G. Venanzoni, e-mail: Graziano.Venanzoni@lnf.infn.it

- ^a*Dipartimento di Fisica dell'Università e Sezione INFN, Bari, Italy.*
- ^b*Permanent address: Institute of High Energy Physics, CAS, Beijing, China.*
- ^c*Laboratori Nazionali di Frascati dell'INFN, Frascati, Italy.*
- ^d*Institut für Experimentelle Kernphysik, Universität Karlsruhe, Germany.*
- ^e*Dipartimento di Fisica dell'Università e Sezione INFN, Lecce, Italy.*
- ^f*Permanent address: Institute for Theoretical and Experimental Physics, Moscow, Russia.*
- ^g*Dipartimento di Scienze Fisiche dell'Università "Federico II" e Sezione INFN, Napoli, Italy.*
- ^h*Permanent address: Budker Institute of Nuclear Physics, Novosibirsk, Russia.*
- ⁱ*Dipartimento di Fisica dell'Università e Sezione INFN, Pisa, Italy.*
- ^j*Dipartimento di Energetica dell'Università "La Sapienza", Roma, Italy.*
- ^k*Dipartimento di Fisica dell'Università "La Sapienza" e Sezione INFN, Roma, Italy.*
- ^l*Dipartimento di Fisica dell'Università "Tor Vergata" e Sezione INFN, Roma, Italy.*
- ^m*Dipartimento di Fisica dell'Università "Roma Tre" e Sezione INFN, Roma, Italy.*
- ⁿ*Physics Department, State University of New York at Stony Brook, USA.*
- ^o*Physics Department, University of Virginia, USA.*

Abstract

We have measured the cross section $\sigma(e^+e^- \rightarrow \pi^+\pi^-\gamma)$ at an energy $W = m_\phi = 1.02$ GeV with the KLOE detector at the electron-positron collider DAΦNE. From the dependence of the cross section on the invariant mass of the two-pion system, we extract $\sigma(e^+e^- \rightarrow \pi^+\pi^-)$ for the mass range $0.35 < s < 0.95$ GeV². From this result, we calculate the pion form factor and the hadronic contribution to the muon anomaly, a_μ .

Key words: Hadronic cross section, initial state radiation, pion form factor, muon anomaly

PACS: 13.40.Gp, 13.60.Hb, 13.66.Bc, 13.66.Jn

1 Hadronic cross section at DAΦNE

1.1 Motivation

The recent precision measurement of the muon anomaly a_μ at the Brookhaven National Laboratory [1] has led to renewed interest in an accurate measurement of the cross section for e^+e^- annihilation into hadrons. Contributions to the photon spectral functions due to quark loops are not calculable for low-hadronic-mass states by perturbative QCD at low energy. However, they can be obtained by connecting the imaginary part of the hadronic piece of the polarization function by unitarity to the cross section for $e^+e^- \rightarrow$ hadrons [2,3]. A dispersion relation can thus be derived, giving the contribution to a_μ as an integral over the hadronic cross section multiplied by a kernel $K(s)$, which behaves approximately like $1/s$:

$$a_\mu^{\text{had}} = \frac{1}{4\pi^3} \int_{4m_\pi^2}^{\infty} \sigma_{e^+e^- \rightarrow \text{hadr}}(s) K(s) ds. \quad (1)$$

The process $e^+e^- \rightarrow \pi^+\pi^-$ below 1 GeV accounts for 62% of the total hadronic contribution [4]. The most recent measurements of $\sigma(e^+e^- \rightarrow \pi^+\pi^-)$ for values of \sqrt{s} between 610 and 961 MeV come from the CMD-2 experiment at VEPP-2M where the quoted systematic error is 0.6% and the contribution of the statistical error on a_μ^{had} is $\sim 0.7\%$ [5,6]. These data, together with τ and e^+e^- data up to 3 GeV, have been used to produce a prediction for comparison with the BNL result [7]. There is however a rather strong disagreement between the a_μ^{had} value obtained using τ decay data after isospin-breaking corrections and $e^+e^- \rightarrow \pi^+\pi^-$ data. Moreover, the $e^+e^- \rightarrow \pi^+\pi^-$ based result disagrees by $\sim 3\sigma$ with the direct measurement of a_μ .

1.2 Radiative Return

Initial state radiation (ISR) is a convenient mechanism that allows one to study $e^+e^- \rightarrow$ hadrons over the entire range from $2m_\pi$ to W , the center of mass energy of the colliding beams. In this case, there are complications from final-state radiation (FSR). For a photon radiated prior to the annihilation of the e^+e^- pair, the mass of the $\pi^+\pi^-$ -system is¹ $m_{\pi^+\pi^-} = \sqrt{W^2 - 2WE_\gamma}$. Instead, for a photon radiated by the final-state pions, the virtual photon coupling to the $\pi^+\pi^-$ pair has a mass W . By counting vertices, the relative probabilities

¹ Neglecting the small momentum of the ϕ .

of ISR and FSR are of the same order. This requires careful estimates of the two processes in order to be able to use the reaction $e^+e^- \rightarrow \pi^+\pi^-\gamma$ to extract $\sigma(e^+e^- \rightarrow \pi^+\pi^-)$. The Karlsruhe theory group has developed the EVA and PHOKHARA Monte Carlo programs which are fundamental to our analysis [8–13]. In particular, the PHOKHARA Monte Carlo simulation has been used to evaluate the contribution for the ISR process (via the radiation function H) in order to derive the hadronic cross section:

$$s_\pi \frac{d\sigma_{\pi^+\pi^-\gamma}}{ds_\pi} = \sigma_{\pi^+\pi^-}(s_\pi)H(s_\pi), \quad (2)$$

where $s_\pi = m_{\pi^+\pi^-}^2$, which coincides with the invariant mass s of the intermediate photon for the case of ISR radiation only. The equation above is correct at leading order if FSR emission can be neglected. The case of NLO terms, with the simultaneous emission of ISR and FSR photons, is discussed in Sec. 3.1.

The present analysis is based on the observation of Ref. [8] that for small polar angle θ_γ of the radiated photon, the ISR process vastly dominates over the FSR process. In the following we restrict ourself to studying the reaction $e^+e^- \rightarrow \pi^+\pi^-\gamma$ with $\theta_\gamma < 15^\circ$ or $\theta_\gamma > 165^\circ$. For small s_π , the di-pion system recoiling against a small angle photon will result in one or both pions being lost at small angle as well. We are therefore limited to measuring $\sigma(\pi^+\pi^-)$ for $\sqrt{s_\pi} > 550$ MeV. In the future extension of this work we will be able to measure the cross section near threshold. This is very important, since there are no good measurements of $\sigma(\pi^+\pi^-)$ at low masses, which weigh strongly in the estimate of a_μ^{had} .

2 Measurement of $\sigma(e^+e^- \rightarrow \pi^+\pi^-\gamma)$

2.1 Signal selection

The KLOE detector consists mainly of a high resolution drift chamber with transverse momentum resolution $\sigma_{p_T}/p_T \leq 0.4\%$ [14] and an electromagnetic calorimeter with energy resolution $\sigma_E/E = 5.7\%/\sqrt{E(\text{GeV})}$ [15]. In the current analysis, we have concentrated on events in which the pions are emitted at polar angles θ_π between 50° and 130° . The direction and energy of the photon is reconstructed from the pion tracks by closing the kinematics; explicit photon detection is not required. As a consequence, a requirement on the di-pion production angle $\theta_{\pi\pi}$ smaller than 15° (or greater than 165°) is performed instead of a requirement on the photon angle θ_γ . The acceptance regions are shown in Fig. 1, left. These specific acceptance requirements reduce background contamination and the relative contribution of final-state

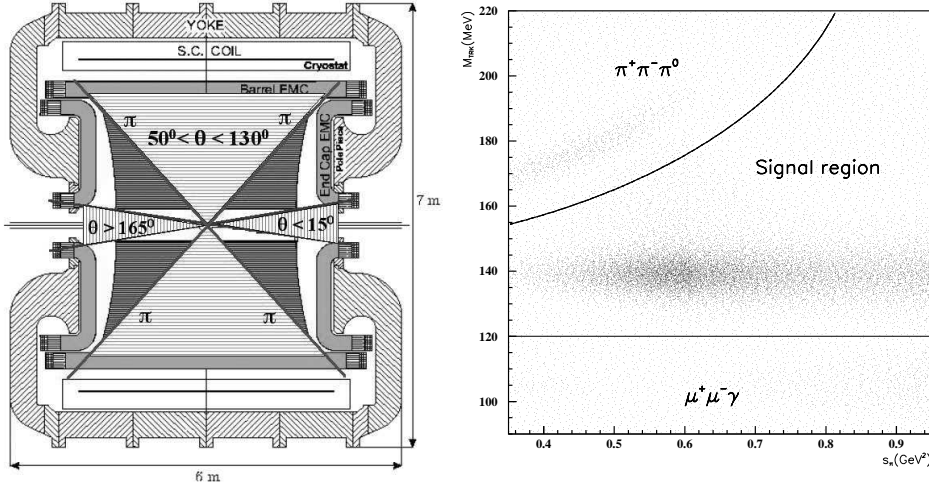


Fig. 1. Left: schematic view of the KLOE detector with the angular acceptance regions for pions (*horizontally hatched area*) and photons (*vertically hatched area*). The photon angle is evaluated from the two pion tracks. Right: 2-dimensional requirement in the plane of $m_{\text{trk}}/\text{MeV}$ and s_{π}/GeV^2 .

radiation from the pions to very low levels [16]. It will be shown in the following that an efficient and nearly background free signal selection can be done without explicit photon tagging.

The selection of $e^+e^- \rightarrow \pi^+\pi^-\gamma$ events is performed with the following steps:

- *Detection of two charged tracks connected to a vertex*: Two charged tracks with polar angles between 50° and 130° connected to a vertex in the fiducial volume, $R_{xy} < 8$ cm, $|z| < 7$ cm, are required. Additional requirements on transverse momentum, $p_T > 160$ MeV, and on longitudinal momentum, $|p_z| > 90$ MeV, reject spiralling tracks and ensure good reconstruction conditions.
- *Identification of pion tracks*: Separation of pions from electrons is performed using a PID method based on approximate likelihood estimators. These estimators are based on the comparison of time-of-flight versus momentum and on the shape and energy deposition of the calorimeter clusters produced by charged tracks. The functions have been built using control samples of $\pi^+\pi^-\pi^0$ and $e^+e^-\gamma$ events in data, in order to obtain the calorimeter response for pions and electrons. An event is selected as signal if at least one of the two tracks is identified as a pion. In this way, the content of $e^+e^-\gamma$ events in the signal sample is drastically reduced, while the efficiency for retaining $\pi^+\pi^-\gamma$ events is still very high ($> 98\%$).
- *Requirement on the track mass*: The track mass (m_{trk}) is a kinematic variable corresponding to the mass of the charged tracks under the hypothesis that the final state consists of two particles with the same mass and one photon. It is calculated from the reconstructed momenta of the π^+ and π^-

(\vec{p}_+, \vec{p}_-) and the center-of-mass energy W . Requiring a value larger than 120 MeV rejects $\mu^+\mu^-\gamma$ events, while in order to reject $\pi^+\pi^-\pi^0$ events, an s_π -dependent requirement is used (see Fig. 1, right).

- *Requirement on the di-pion angle $\theta_{\pi\pi}$* : The aforementioned requirement on the di-pion angle $\theta_{\pi\pi} < 15^\circ$ or $> 165^\circ$ and $50^\circ < \theta_\pi < 130^\circ$ is performed.

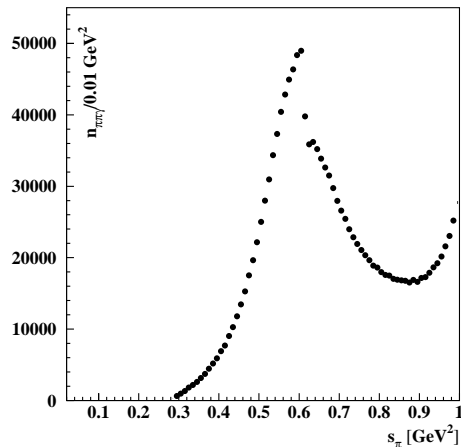


Fig. 2. Distribution of counts as a function of s_π , in bins of 0.01 GeV^2 , after applying the acceptance and selection requirements. $\mathcal{L} = 141.4 \text{ pb}^{-1}$; data from 2001.

The data used for the analysis were taken from July to December 2001, yielding an integrated luminosity of $\mathcal{L} = 141.4 \text{ pb}^{-1}$. After the selection requirements mentioned above, we find 1.555×10^6 events, corresponding to $\simeq 11000 \text{ events/pb}^{-1}$. Figure 2 shows the distribution of the $\pi^+\pi^-\gamma$ events in bins of 0.01 GeV^2 for s_π . The ρ peak and the $\rho - \omega$ interference structure are clearly visible, even without unfolding the spectrum from the detector resolution, demonstrating the excellent momentum resolution of the KLOE detector. To obtain the cross section for $0^\circ < \theta_\pi < 180^\circ$ and $\theta_{\pi\pi} < 15^\circ$, $\theta_{\pi\pi} > 165^\circ$ we subtract the residual background from this spectrum and divide by the selection efficiency, acceptance, and integrated luminosity:

$$\frac{d\sigma_{\pi^+\pi^-\gamma}}{ds_\pi} = \frac{\Delta N_{\text{Obs}} - \Delta N_{\text{Bkg}}}{\Delta s_\pi} \frac{1}{\epsilon_{\text{Sel}}\epsilon_{\text{Acc}}} \frac{1}{\int \mathcal{L} dt}. \quad (3)$$

The background subtraction, the evaluation of the selection efficiency and the acceptance, the measurement of the integrated luminosity, and the unfolding of the experimental resolution on s_π (omitted from Eq. (3) for clarity) are discussed below. Detailed information on all the aspects of the analysis is available in [17].

2.2 Background subtraction

After applying the requirements on the fiducial volume, the likelihood, and m_{trk} , a residual background of $e^+e^-\gamma$, $\mu^+\mu^-\gamma$, and $\pi^+\pi^-\pi^0$ events remains. The population of signal and background events in the $[s_\pi, m_{\text{trk}}]$ plane is illustrated in Fig. 1, right. Background from $e^+e^-\gamma$ and $\mu^+\mu^-\gamma$ events is concentrated at low values of m_{trk} . The amount of background in the signal region is obtained by fitting the m_{trk} spectra of the selected events (except for the m_{trk} requirement) in slices of s_π . The m_{trk} spectra for signal and $\mu^+\mu^-\gamma$ events are obtained from Monte Carlo simulation, while for $e^+e^-\gamma$ events, m_{trk} is obtained directly from data, using a dedicated sample of 152 pb^{-1} . An example of such a fit to determine the background fraction for $\mu^+\mu^-\gamma$ events is shown in Fig. 3, left. Background from $\pi^+\pi^-\pi^0$ events appears at higher m_{trk} values and the missing mass $m_{\text{miss}}^2 = (p_\phi - p_+ - p_-)^2$, peaks at $m_{\pi^0}^2$. The number of $\pi^+\pi^-\pi^0$ events in the signal region is obtained by fitting the m_{miss} distribution with the shapes obtained from the Monte Carlo simulation; an example is shown in Fig. 3, right. The shape of the background distribution is well repro-

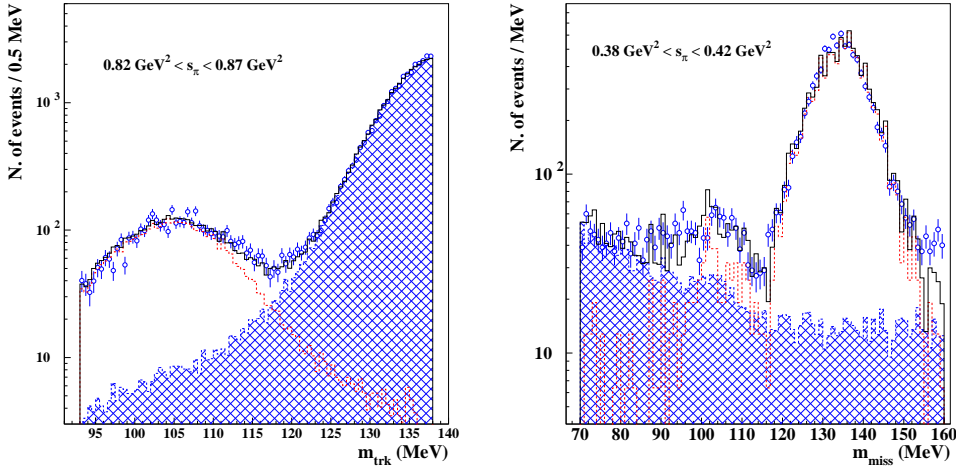


Fig. 3. Left: fit of the mass peak for muons. Right: π^0 mass fit. These fits are used to estimate the $\mu^+\mu^-\gamma$ and $\pi^+\pi^-\pi^0$ backgrounds to the $\pi^+\pi^-\gamma$ channel. Points are data, solid line is Monte Carlo simulation. Dashed line and hashed area represent the Monte Carlo evaluation of background ($\mu^+\mu^-\gamma$ in the left plot and $\pi^+\pi^-\pi^0$ in the right one) and $\pi^+\pi^-\gamma$ contributions, respectively.

duced by the Monte Carlo simulation, ensuring that systematic uncertainties are smaller than the fit errors, which are considered as systematic errors of the procedure.

The contribution of all backgrounds to the observed signal is below 2% above 0.5 GeV^2 , while it increases up to $\sim 10\%$ at $s_\pi = 0.35 \text{ GeV}^2$. Other possible

sources of background for which the contributions have been evaluated are the process $e^+e^- \rightarrow e^+e^-\pi^+\pi^-$ with the electrons emitted along the beam pipe [18] and the NLO corrections to the FSR in the process $e^+e^- \rightarrow \mu^+\mu^-\gamma$ [19]. The systematic uncertainties associated with the background estimates for all these sources have been added in quadrature; the results are shown in Table 2.

2.3 The selection efficiency ϵ_{Sel}

The selection efficiency is the product of the efficiencies associated with the trigger, the event reconstruction, the background filtering and the track mass requirement: in

- *Trigger efficiency:* Events in the $\pi^+\pi^-\gamma$ sample must satisfy the calorimeter trigger, *i.e.*, there must be at least two trigger sectors with energy deposition above threshold (for details on the KLOE trigger see [20]). The trigger also includes a cosmic-ray veto: events with energy deposition above a certain threshold in the outermost layer of the calorimeter are rejected on-line. While the calorimeter trigger itself is rather efficient for signal events ($> 95\%$), the cosmic-ray veto rejects a significant fraction of $\pi^+\pi^-\gamma$ events since such events mimic cosmic rays. The cosmic-ray veto inefficiency is on the level of few percent at small values of $s_\pi < 0.4\text{GeV}^2$ but reaches up to 30% at $s_\pi = 0.95\text{GeV}^2$. The overall trigger efficiency, including the effect of the cosmic-ray veto, was evaluated from the probability for single pions to fire trigger sectors in $\pi^+\pi^-\gamma$ events wherein part of the event could be ascertained to have satisfied the trigger alone. The fractional uncertainty associated with this procedure was estimated to be $\delta\epsilon_{\text{TRG}}(s_\pi) = [\exp(0.43 - 4.9s_\pi[\text{GeV}^2]) + 0.08]$ (expressed in percent), and is dominated by the systematics of establishing the correct track-to-trigger sector association.
- *Background filter efficiency:* During reconstruction, an offline filtering procedure identifies and rejects background events as soon as they have been reconstructed in the calorimeter [21]. The efficiency of this filter has been studied using a dedicated sample of $\pi^+\pi^-\gamma$ events that were rejected by the filter itself. Since the filtering procedure is very sensitive to the presence of accidental clusters in the electromagnetic calorimeter, the efficiency of this filter was parametrized as a function of the background conditions during data taking and averaged over time. The filter efficiency was found to be uniform in s_π and 96.6% on average, with a flat systematic error of 0.6%.
- *Tracking efficiency:* The tracking efficiency (96% and uniform in s_π) was evaluated using $\pi^+\pi^-\pi^0$ and $\pi^+\pi^-$ -events identified by calorimeter information plus the presence of one fitted track. The single-track efficiency as a function of p_π and θ_π was compared with Monte Carlo simulation; the difference, on the order of 0.3% and flat in momentum, was taken as the

systematic error of this procedure.

- *Vertex efficiency*: The efficiency of the vertex finding algorithm has been evaluated via Monte Carlo simulation and checked with a sample of $\pi^+\pi^-\pi^0$ and $\pi^+\pi^-\gamma$ events obtained from data. The absolute vertex efficiency at low energies is 91% and is increasing up to 97% at high values of s_π . An uncertainty of 0.3%, uniform in s_π , is taken as the contribution to the systematic error for this efficiency.
- *Pion identification*: The efficiency for π/e separation has been evaluated by selecting $\pi^+\pi^-\gamma$ events on the basis of one track and examining the distribution of the likelihood estimator for the other one. In the analysis, only one track is required to satisfy the likelihood requirement, for which the efficiency is $> 99.9\%$. Therefore, no correction for the inefficiency on pion identification needs to be applied; the contribution to the systematic error is taken to be 0.1%.
- *Track mass*: The efficiency of the m_{trk} requirement is obtained as a by-product of the background evaluation; the result of the fit provides the efficiency in each s_π bin. However, this efficiency depends upon the treatment of multi-photon processes in the Monte Carlo simulation. The m_{trk} efficiency has been obtained with our reference Monte Carlo simulation, which uses PHOKHARA. To check the efficiency determination we have compared PHOKHARA with BABAYAGA [22], which is the generator used for the luminosity measurement. In the latter generator, ISR is treated using the parton-shower approach. The resulting value for the m_{trk} efficiency differs from that evaluated with PHOKHARA by 0.2%. Effects on the efficiency from the simultaneous emission of an ISR and a FSR photon are discussed in Sec. 3.1.

2.4 Unfolding of the mass resolution

To obtain $d\sigma_{\pi\pi\gamma}/ds_\pi$ as a function of the true value of s_π , we unfold the mass resolution from the measured s_π distribution. The measured value of $s_{\pi,\text{obs}}$ is related to the true value via the resolution matrix $\mathbf{G}(s_{\pi,\text{true}} - s_{\pi,\text{obs}}|s_{\pi,\text{true}})$, which has been obtained by a Monte Carlo simulation carefully tuned to reproduce the data. The resolution matrix is nearly diagonal, as can be seen in in Fig. 4, left. A comparison of the track-mass distribution for data and Monte Carlo events is shown Fig. 4, right.

Unfolding of the spectrum is performed using GURU [23], an unfolding program based on the singular value decomposition (SVD). We found that the systematic error due to unfolding is dominated by the uncertainty on the value chosen to regularize the procedure itself. Table 3 shows the systematic uncertainty as function of s_π , introduced into the $\pi^+\pi^-\gamma$ spectrum due to the unfolding. These values are taken to be correlated errors, and translate into a

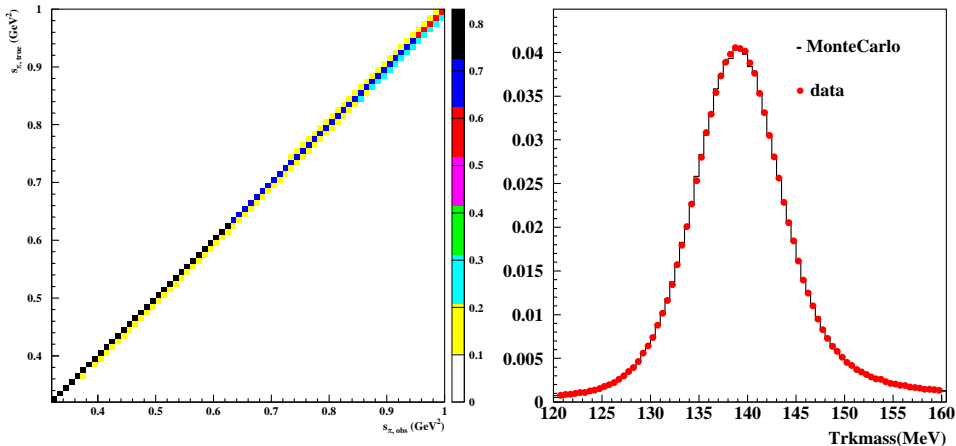


Fig. 4. Left: Smearing matrix representing the correlation between generated ($s_{\pi,\text{true}}$) and reconstructed ($s_{\pi,\text{obs}}$) values for s_{π} ; the high precision of the DC results in an almost diagonal matrix. Right: track mass distribution expected from the Monte Carlo simulation compared to the experimental one.

0.2% systematic uncertainty on a_{μ} .²

In addition, the unfolding procedure correlates the statistical errors in the $\pi^+\pi^-\gamma$ spectrum (see also Sec. 4).

2.5 Acceptance correction

After all corrections discussed above, we obtain the spectrum for $\pi^+\pi^-\gamma$ events defined by the acceptance requirements $50^\circ < \theta_{\pi} < 130^\circ$, $\theta_{\pi\pi} < 15^\circ$ or $\theta_{\pi\pi} > 165^\circ$, $p_T > 160$ MeV, and $p_z > 90$ MeV. To derive the cross section for the process $e^+e^- \rightarrow \pi^+\pi^-\gamma$ with $\theta_{\pi\pi} < 15^\circ$ or $\theta_{\pi\pi} > 165^\circ$, the effects of the other requirements on the momentum and polar angle of the pions have been evaluated using PHOKHARA. The systematic error of 0.3% on the acceptance fraction has been estimated by a comparison of data and Monte Carlo distributions.

2.6 Luminosity measurement

The integrated luminosity is measured with the KLOE detector itself using very-large-angle Bhabha (VLAB) events. The effective Bhabha cross section at large angles ($55^\circ < \theta_{+,-} < 125^\circ$) is about 430 nb. This cross section is

² This value should be considered as an overestimate of the real effect introduced by the unfolding procedure on a_{μ} , as discussed in [17].

large enough so that the statistical error on the luminosity measurement is negligible. The number of VLAB candidates, N_{VLAB} , is counted and normalized to the effective Bhabha cross section, $\sigma_{\text{VLAB}}^{\text{MC}}$, obtained by Monte Carlo simulation, after subtraction of the background, δ_{Bkg} :

$$\int \mathcal{L} dt = \frac{N_{\text{VLAB}}(\theta_i)}{\sigma_{\text{VLAB}}^{\text{MC}}(\theta_i)} (1 - \delta_{\text{Bkg}}). \quad (4)$$

The precision of the luminosity measurement depends on the correct inclusion of higher-order terms in computing the Bhabha cross section. We use the Bhabha event generator BABAYAGA [22], which has been developed explicitly for DAΦNE. In BABAYAGA, QED radiative corrections are taken into account in the framework of the parton-shower method. The precision quoted is 0.5%. The result for the effective Bhabha cross section has been compared with that from BHAGENF [24, 25], a full order- α event generator. We find agreement to better than 0.2%.

VLAB events are selected with requirements on variables that are well reproduced by the KLOE Monte Carlo simulation. The electron and positron polar angle requirements, $55^\circ < \theta_{+,-} < 125^\circ$, are based on the calorimeter clusters, while the energy requirements, $E_{+,-} > 400$ MeV, are based on drift chamber information. The background from $\mu^+\mu^-(\gamma)$, $\pi^+\pi^-(\gamma)$ and $\pi^+\pi^-\pi^0$ events is well below 1% and is subtracted. All selection efficiencies (trigger, EmC cluster, DC tracking) are $> 99\%$ as obtained by Monte Carlo simulation and confirmed with data. We obtain excellent agreement between the experimental distributions ($\theta_{+,-}$, $E_{+,-}$) and those obtained from Monte Carlo simulation, as seen in Fig. 5. Finally, corrections are applied on a run-by-run basis for fluctuations in the center-of-mass energy of the machine and in the detector calibrations. The experimental uncertainty in the acceptance due to all these effects is 0.3%. We assign a total systematic error on the luminosity of $\delta\mathcal{L} = 0.5\%_{\text{th}} \oplus 0.3\%_{\text{exp}}$. The luminosity measurement is independently checked using $e^+e^- \rightarrow \gamma\gamma$ events. We find agreement to within 0.2%.

2.7 $\pi^+\pi^-\gamma$ cross section

Our results for the differential cross section $d\sigma(e^+e^- \rightarrow \pi^+\pi^-\gamma)/ds_\pi$ with $0^\circ < \theta_\pi < 180^\circ$ and $\theta_{\pi\pi} < 15^\circ$, $\theta_{\pi\pi} > 165^\circ$ are plotted in Fig. 6, left, and are presented in numerical form in the second column of Table 1.

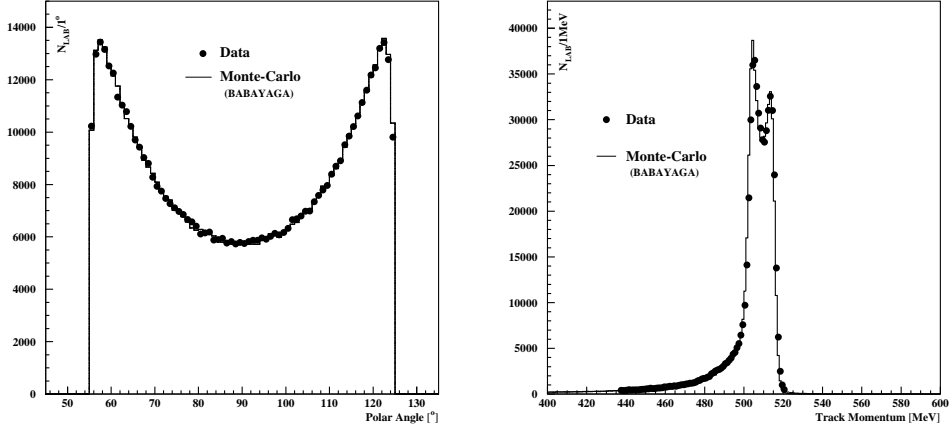


Fig. 5. Data-Monte Carlo comparison of the $\theta_{+,-}$ (left) and $E_{+,-}$ (right) distributions for Bhabha events selected at large angle as described in the text.

3 Extraction of $\sigma(e^+e^- \rightarrow \pi^+\pi^-)$ and $|F_\pi(s)|^2$

In order to extract the $e^+e^- \rightarrow \pi^+\pi^-$ cross section, the radiation function H is needed (see Eq. [2]). This function is obtained from PHOKHARA, setting $F_\pi(s) = 1$ and *switching off* the vacuum polarization of the intermediate photon in the generator. Applying Eq. (2), and taking the FSR contribution into account, as described in the following section, the hadronic cross section as a function of the invariant mass of the virtual photon, $s = m_{\gamma^*}^2$, is obtained, as shown in Fig.6, right.

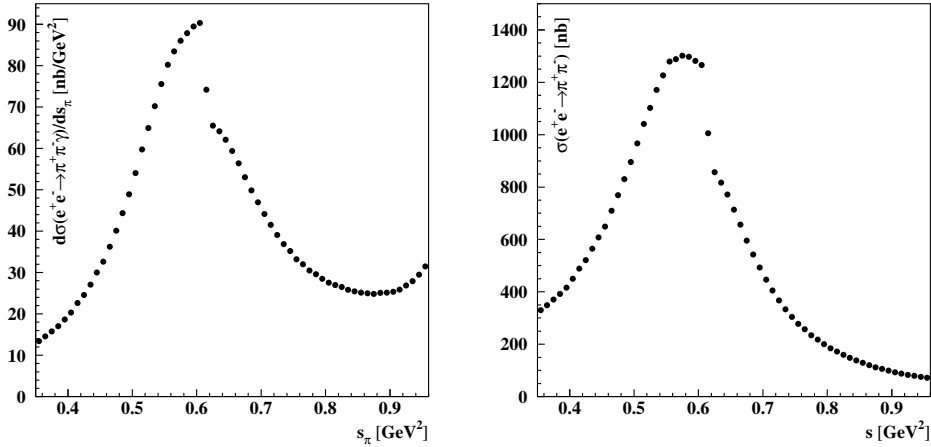


Fig. 6. Left: differential cross section for the $e^+e^- \rightarrow \pi^+\pi^-\gamma$ process, inclusive in θ_π and with $\theta_{\pi\pi} < 15^\circ$ ($\theta_{\pi\pi} > 165^\circ$). Right: cross section for $e^+e^- \rightarrow \pi^+\pi^-$.

3.1 FSR corrections

Events with one or more photons emitted by the pions (FSR) without any photons in the initial state must be considered as a background to our measurement. Our event selection strongly suppresses the contribution of such events to well below 1% over the entire range of s_π .

However, events with the simultaneous emission of one photon from the initial state and one photon from the final state must be included in our selection in order for the $e^+e^- \rightarrow \pi^+\pi^-$ cross section to be inclusive with respect to FSR (see Ref. [7] for details). More specifically, since the radiator function H only describes the ISR part of the radiative corrections, the process $e^+e^- \rightarrow \gamma^* \rightarrow \pi^+\pi^-\gamma_{\text{ISR}}(\gamma_{\text{FSR}})$, with one photon from initial state and possibly another from the final state, corresponds to $e^+e^- \rightarrow \gamma^* \rightarrow \pi^+\pi^-(\gamma_{\text{FSR}})$ after the division by H .

Therefore,

$$\sigma(e^+e^- \rightarrow \pi^+\pi^-(\gamma_{\text{FSR}})) = \frac{\pi\alpha^2}{3s} \beta_\pi^3 \frac{d\sigma^{\pi\pi\gamma}(\gamma_{\text{FSR}})}{c_{s_\pi,s} A(s) d\sigma^{\pi\pi\gamma}(F_\pi = 1)}, \quad (5)$$

where $d\sigma^{\pi\pi\gamma}(F_\pi = 1)$ is the NLO cross section for $e^+e^- \rightarrow \pi^+\pi^-\gamma$ (initial state radiation only), inclusive in $\theta_{\pi\pi}$ and θ_π under the assumption of pointlike pions, and corresponds to the quantity H of Eq. (2); $A(s)$ is the fraction of $\pi^+\pi^-\gamma_{\text{ISR}}(\gamma_{\text{FSR}})$ events selected by the angular cuts $\theta_{\pi\pi} < 15^\circ$ or $\theta_{\pi\pi} > 165^\circ$, $50^\circ < \theta_\pi < 130^\circ$ as a function of the invariant mass s of the virtual photon; and $c_{s_\pi,s}$ is a correction which must be applied due to the fact that, in the presence of simultaneous emission of initial- and final-state photons, s_π is not identical to s , as it is in the case of ISR only. Both $A(s)$ and $c_{s_\pi,s}$ have been obtained using the PHOKHARA Monte Carlo generator [13], which simulates the simultaneous emission of initial- and final-state photons.

Note that $\sigma(e^+e^- \rightarrow \pi^+\pi^-)$ is obtained under the assumptions of (i) radiation emission from pointlike pions (the scalar QED model for FSR) and (ii) factorization, *i.e.*, the absence of interference effects between the initial and final states [13]. We have used an alternative method which provides some test of the validity of the factorization ansatz and a valuable cross-check of the entire analysis. In this method, we correct the observed $\pi\pi\gamma$ cross section for the relative amount of FSR expected from PHOKHARA, obtaining, in this way, a cross section that corresponds to ISR emission only. Next, we perform the event analysis, in which the acceptance correction and track-mass efficiency are taken from a Monte Carlo sample in which only ISR events are simulated. After dividing by the radiator function H , the full (*i.e.*, real and virtual) FSR corrections to the cross section $e^+e^- \rightarrow \pi^+\pi^-$ are applied [26, 27].

The results for $\sigma(e^+e^- \rightarrow \pi^+\pi^-)$ obtained with the two methods agree to within $\approx 0.2\%$. Taking into account the additional uncertainty arising from the assumption of radiation from pointlike pions, we assign an error of 0.3% due to the FSR corrections discussed in this section.

3.2 Vacuum polarization corrections

To obtain the pion form factor and the *bare* cross section, leptonic and hadronic vacuum polarization contributions in the photon propagator must be subtracted. This can be done by correcting the cross section for the running of α as follows:

$$\sigma_{\text{bare}} = \sigma_{\text{dressed}} \left(\frac{\alpha(0)}{\alpha(s)} \right)^2. \quad (6)$$

While the leptonic contribution $\Delta\alpha_{\text{lep}}(s)$ can be analytically calculated, for the hadronic contribution, $\Delta\alpha_{\text{had}}(s)$, we have used $\sigma_{\text{had}}(s)$ values measured previously [28].

The pion form factor $|F_\pi(s)|^2$ obtained after additional subtraction of FSR is shown in Fig. 7. Note that in this case, since the FSR effects have been removed, $s_\pi = s$.

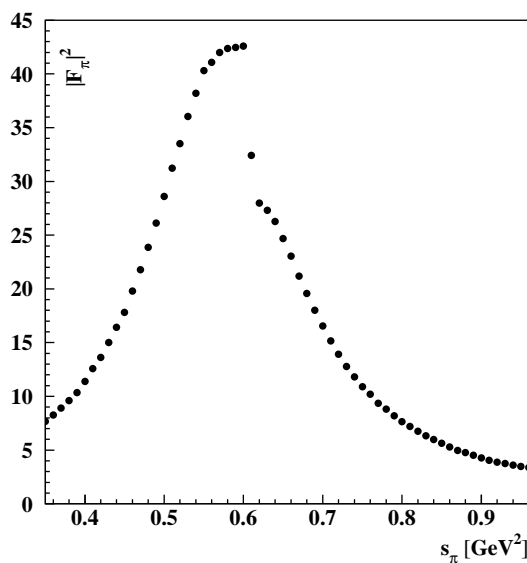


Fig. 7. Pion form factor.

4 Results

Our results are summarized in Table 1, which lists:

- the differential cross section $d\sigma(e^+e^- \rightarrow \pi^+\pi^-\gamma)/ds_\pi$ as a function of the invariant mass of the di-pion system, s_π , in the angular region $\theta_{\pi\pi} < 15^\circ$ or $\theta_{\pi\pi} > 165^\circ$, $0^\circ < \theta_\pi < 180^\circ$;
- the physical cross section $\sigma(e^+e^- \rightarrow \pi^+\pi^-)$, which includes FSR and vacuum polarization effects, as a function of the invariant mass of the virtual photon s ;
- the pion form factor with FSR and vacuum polarization effects removed, as a function of s (equal to s_π in this case).

The errors given in Table 1 are statistical only, while the common systematic error is shown in Tables 2, 3, and 4. It should be noted that the statistical errors account only for the diagonal elements of the covariance matrix. The bin-by-bin errors are correlated as a result of the unfolding procedure; for error propagation, as for example in the calculation of a_μ (see below), the covariance matrix must be used.

The unfolding procedure is necessary in order to provide a table of data points at meaningful values of s_π . However, the procedure itself introduces additional systematic uncertainties because of the numerical instability of the problem. For the comparison of our data with a specific theoretical prediction, we strongly recommend fitting our observed spectrum with a convolution of the theoretical curve and the detector response matrix, which is available upon request [29].

The $\sigma(e^+e^- \rightarrow \pi^+\pi^-)$ cross section, divided by the vacuum polarization, has been used to evaluate the contribution to a_μ^{had} due to the $\pi^+\pi^-$ channel in the energy range $0.35 < s_\pi < 0.95$ GeV². The resulting value (in 10^{-10} units) is

$$a_\mu^{\pi\pi}(0.35, 0.95) = 388.7 \pm 0.8_{\text{stat}} \pm 3.5_{\text{syst}} \pm 3.5_{\text{th}}. \quad (7)$$

The various contributions to the systematic error on a_μ are listed in Table 5.

5 Conclusions

We have measured the cross section for the process $e^+e^- \rightarrow \pi^+\pi^-\gamma$ with the pion system emitted at small polar angles with respect to the electron or positron beam ($\theta_{\pi\pi} < 15^\circ$, $\theta_{\pi\pi} > 165^\circ$) in the energy region $0.35 < s_\pi < 0.95$ GeV². Using Eq. (2), we have derived the cross section for the process

$e^+e^- \rightarrow \pi^+\pi^-$, as listed in Table 1. These values, corrected for the vacuum polarization, can be used to derive part of the hadronic contribution to the muon anomalous magnetic moment with a negligible statistical error and with a systematic error of $0.9\%(\text{exp}) \oplus 0.9\%(\text{th})$.

s_π GeV ²	$\pi^+\pi^-\gamma$ nb/GeV ²	$\pi^+\pi^-$ nb	$ F_\pi(s) ^2$	s_π GeV ²	$\pi^+\pi^-\gamma$ nb/GeV ²	$\pi^+\pi^-$ nb	$ F_\pi(s) ^2$
0.35	13.40±0.24	330±7	7.68±0.16	0.65	59.40±0.28	714±4	24.69±0.15
0.36	14.59±0.24	349±7	8.26±0.16	0.66	56.38±0.24	657±4	23.05±0.14
0.37	15.78±0.24	370±7	8.92±0.16	0.67	53.04±0.23	595±4	21.18±0.13
0.38	17.04±0.24	392±6	9.60±0.16	0.68	49.87±0.26	543±4	19.57±0.13
0.39	18.63±0.23	416±6	10.35±0.15	0.69	46.98±0.22	493.2±3.1	18.02±0.11
0.40	20.34±0.27	450±7	11.40±0.17	0.70	44.16±0.21	447.0±2.9	16.54±0.11
0.41	22.64±0.24	489±6	12.59±0.16	0.71	41.54±0.19	405.0±2.6	15.17±0.10
0.42	24.56±0.27	521±7	13.63±0.18	0.72	39.05±0.21	367.1±2.6	13.92±0.10
0.43	27.07±0.28	564±7	15.01±0.18	0.73	36.87±0.17	333.3±2.2	12.78±0.08
0.44	29.99±0.27	608±7	16.43±0.18	0.74	35.20±0.18	304.6±2.0	11.81±0.08
0.45	32.65±0.28	649±7	17.82±0.19	0.75	33.22±0.16	277.8±1.8	10.89±0.07
0.46	36.24±0.27	710±7	19.79±0.18	0.76	31.99±0.16	257.2±1.7	10.19±0.07
0.47	40.10±0.29	769±7	21.78±0.20	0.77	30.51±0.17	233.8±1.7	9.37±0.07
0.48	44.34±0.31	830±7	23.86±0.20	0.78	29.60±0.16	217.7±1.6	8.82±0.06
0.49	48.94±0.28	895±7	26.11±0.20	0.79	28.52±0.13	200.3±1.3	8.20±0.05
0.50	54.1±0.4	967±8	28.60±0.23	0.80	27.53±0.14	184.5±1.3	7.63±0.05
0.51	59.77±0.32	1041±7	31.23±0.22	0.81	27.00±0.14	172.1±1.2	7.20±0.05
0.52	64.93±0.32	1102±7	33.50±0.22	0.82	26.48±0.13	160.0±1.1	6.76±0.05
0.53	70.24±0.35	1171±8	36.05±0.23	0.83	25.84±0.15	148.4±1.1	6.33±0.05
0.54	75.6±0.4	1226±8	38.20±0.26	0.84	25.45±0.13	138.5±1.0	5.97±0.04
0.55	80.2±0.4	1279±8	40.32±0.24	0.85	25.16±0.13	129.2±0.9	5.63±0.04
0.56	83.47±0.35	1288±7	41.07±0.24	0.86	24.96±0.12	120.3±0.8	5.29±0.04
0.57	86.06±0.34	1302±7	41.98±0.23	0.87	24.81±0.15	111.8±0.9	4.97±0.04
0.58	87.85±0.34	1297±7	42.36±0.23	0.88	25.09±0.14	106.3±0.8	4.774±0.035
0.59	89.5±0.4	1282±7	42.46±0.24	0.89	25.17±0.12	99.5±0.7	4.516±0.030
0.60	90.31±0.35	1266±7	42.58±0.23	0.90	25.37±0.13	93.1±0.6	4.269±0.030
0.61	74.20±0.35	1006±6	32.43±0.20	0.91	25.86±0.12	87.6±0.6	4.059±0.027
0.62	65.49±0.28	857±5	27.99±0.16	0.92	26.87±0.14	83.0±0.6	3.886±0.026
0.63	64.14±0.28	817±5	27.32±0.16	0.93	27.94±0.14	79.1±0.5	3.741±0.025
0.64	62.09±0.26	772±4	26.27±0.15	0.94	29.49±0.16	75.3±0.5	3.599±0.025

Table 1

Cross sections $d\sigma(e^+e^- \rightarrow \pi^+\pi^-\gamma)/ds_\pi$, $\sigma(e^+e^- \rightarrow \pi^+\pi^-)$ and the pion form factor in 0.01 GeV² intervals where the value given indicates the lower bound. Note that while the $\pi^+\pi^-\gamma$ cross section is given as a function of s_π , the $\pi\pi$ cross section and $|F_\pi|^2$ are given as functions of the invariant mass s of the intermediate photon γ^* .

s (GeV ²)	0	1	2	3	4	5	6	7	8	9
0.3...						0.8	0.7	0.6	0.6	0.5
0.4...	0.5	0.4	0.4	0.4	0.4	0.4	0.4	0.4	0.4	0.4
0.5...	0.3	0.3	0.3	0.3	0.3	0.3	0.3	0.3	0.3	0.3
0.6...	0.3	0.3	0.3	0.3	0.3	0.3	0.3	0.3	0.3	0.3
0.7...	0.3	0.2	0.3	0.3	0.3	0.3	0.3	0.2	0.2	0.2
0.8...	0.2	0.2	0.2	0.2	0.2	0.2	0.2	0.2	0.2	0.2
0.9...	0.2	0.2	0.2	0.2	0.2					

Table 2

Bin-by-bin correlated systematic error in % due to background subtraction in 0.01 GeV² intervals. The indicated values for s represent the lower bin edge.

s (GeV ²)	0.58	0.59	0.6	0.61	0.62	0.63	0.64	0.65
δ_{unf}	0.4	0.9	1.4	3.6	0.9	0.8	0.5	0.4

Table 3

Bin-by-bin correlated systematic error in % on $d\sigma(e^+e^- \rightarrow \pi^+\pi^-\gamma)/ds_\pi$ and $\sigma(e^+e^- \rightarrow \pi^+\pi^-)$ due to unfolding in 0.01 GeV² intervals. The indicated values for s represent the lower bin edge.

	$\sigma_{\pi\pi\gamma}$	$\sigma_{\pi\pi}$	$ F_\pi ^2$
Acceptance	0.3 % flat in s_π		
Trigger	$\exp(0.43 - 4.9s_\pi[\text{GeV}^2])$ % + 0.08 %		
Reconstruction Filter	0.6 % flat in s_π		
Tracking	0.3 % flat in s_π		
Vertex	0.3 % flat in s_π		
Particle ID	0.1 % flat in s_π		
Trackmass	0.2 % flat in s_π		
Luminosity	0.6 % flat in s_π		
FSR resummation	-	0.3 %	
Radiation function ($H(s_\pi)$)	-	0.5 %	
Vacuum Polarization	-	-	0.2 %

Table 4

List of completely bin-by-bin correlated systematic effects.

Acceptance	0.3 %
Trigger	0.3 %
Reconstruction Filter	0.6 %
Tracking	0.3 %
Vertex	0.3 %
Particle ID	0.1 %
Trackmass	0.2 %
Background subtraction	0.3 %
Unfolding	0.2 %
Total exp systematics	0.9 %
Luminosity	0.6 %
Vacuum Polarization	0.2 %
FSR resummation	0.3 %
Radiation function ($H(s_\pi)$)	0.5 %
Total theory systematics	0.9 %

Table 5

List of systematic errors on a_μ .

Future improvements are expected using data taken in 2002, where more stable background conditions and an improved trigger logic should allow for a considerable reduction of the systematic effects stemming from the offline reconstruction filter and the trigger. A similar analysis, applied to events with $\theta_{\pi\pi}$ at larger angles, can probe the energy region down to threshold. Moreover, improved Monte Carlo generators both for the luminosity measurement and for the ISR process are expected to be available in the near future, which will help to reduce the theoretical contribution to the systematic error.

Acknowledgements

We would like to thank Carlo Michel Carloni Calame, Henryk Czyż, Axel Höfer, Stanislaw Jadach, Fred Jegerlehner, Johann Kühn, Guido Montagna, and Germán Rodrigo for numerous useful discussions.

We thank the DAFNE team for their efforts in maintaining low background running conditions and their collaboration during all data-taking. We want to thank our technical staff: G.F. Fortugno for his dedicated work to ensure an efficient operation of the KLOE Computing Center; M. Anelli for his continuous

support to the gas system and the safety of the detector; A. Balla, M. Gatta, G. Corradi, and G. Papalino for the maintenance of the electronics; M.Santoni, G.Paoluzzi, and R.Rosellini for the general support to the detector; C.Pinto (Bari), C.Pinto (Lecce), C.Piscitelli, and A.Rossi for their help during major maintenance periods. This work was supported in part by DOE grant DE-FG-02-97ER41027; by EURODAPHNE, contract FMRX-CT98-0169; by the German Federal Ministry of Education and Research (BMBF) contract 06-KA-957; by Graduiertenkolleg 'H.E. Phys. and Part. Astrophys.' of Deutsche Forschungsgemeinschaft, Contract No. GK 742 and 'Emmy-Noether Research group', Contract No. DE839/1; by INTAS, contracts 96-624, 99-37; and by TARI, contract HPRI-CT-1999-00088.

References

- [1] G. W. Bennett, et al., Phys. Rev. Lett. 92 (2004) 161802.
- [2] L. I. Durand, Phys. Rev. 128 (1962) 441.
- [3] M. Gourdin, de Rafael E., Nucl. Phys. B 10 (1969) 667.
- [4] S. Eidelman, F. Jegerlehner, Z. Phys. C67 (1995) 585.
- [5] R. R. Akhmetshin, et al., Phys. Lett. B 527 (2002) 161.
- [6] R. R. Akhmetshin, et al., Phys. Lett. B 578 (2004) 285.
- [7] M. Davier, S. Eidelman, A. Höcker, Z. Zhang, Eur. Phys. J. C 31 (2003) 503.
- [8] F. Binner, J. H. Kühn, K. Melnikov, Phys. Lett. B 459 (1999) 279.
- [9] G. Rodrigo, A. Gehrmann-De Ridder, M. Guillaume, J. H. Kühn, Eur. Phys. J. C22 (2001) 81.
- [10] G. Rodrigo, H. Czyż, J. H. Kühn, M. Szopa, Eur. Phys. J. C24 (2002) 71.
- [11] J. H. Kühn, G. Rodrigo, Eur. Phys. J. C25 (2002) 215.
- [12] H. Czyż, A. Grzełińska, J. H. Kühn, G. Rodrigo, Eur. Phys. J. C27 (2003) 563.
- [13] H. Czyż, A. Grzełińska, J. H. Kühn, G. Rodrigo, Eur. Phys. J. C33 (2004) 333.
- [14] M. Adinolfi, et al., The tracking detector of the KLOE experiment, Nucl. Instrum. Meth. A 488 (2002) 51.
- [15] M. Adinolfi, et al., The KLOE electromagnetic calorimeter, Nucl. Instrum. Meth. A 482 (2002) 364.
- [16] G. Cataldi, A. Denig, W. Kluge, S. Müller, G. Venanzoni, Frascati Physics Series XVI (2000) 569.

- [17] A. Denig, et al., Measurement of $\sigma(e^+e^- \rightarrow \pi^+\pi^-\gamma)$ and extraction of $\sigma(e^+e^- \rightarrow \pi^+\pi^-)$ below 1 GeV with the KLOE detector, KLOE Note 192 (2004).
URL <http://www.lnf.infn.it/kloe/pub/knote/kn192.ps>
- [18] H. Czyż, E. Nowak, Acta Phys. Polon. B34 (2003) 5231.
- [19] H. Czyż, A. Grzebińska, J. H. Kühn, G. Rodrigo, [hep-ph/0404078] (2004).
- [20] M. Adinolfi, et al., The trigger system of the KLOE experiment, Nucl. Instrum. Meth. A492 (2002) 134.
- [21] F. Ambrosino, et al., Data handling, reconstruction, and simulation for the KLOE experiment, [physics/0404100], In press Nucl. Instrum. Meth. (2004).
- [22] C. M. Carloni Calame, et al., Nucl. Phys. B 584 (2000) 459.
- [23] A. Höcker, V. Kartvelishvili, Nucl. Instrum. Meth. A372 (1996) 469.
- [24] F. A. Berends, R. Kleiss, Nucl. Phys. B 228 (1983) 537.
- [25] E. Drago, G. Venanzoni, A Bhabha Generator for DAΦNE including radiative corrections and ϕ resonance, INFN/AE-97/48 (1997).
- [26] J. Schwinger, in: Particles, Sources and Fields, Vol.3, Addison-Wesley, Redwood City, USA, 1989, p. 99.
- [27] A. Höfer, J. Gluza, F. Jegerlehner, Eur. Phys. J. C24 (2002) 51.
- [28] URL <http://www-zeuthen.desy.de/~fjeger/alphaQEDn.uu>
- [29] The covariance matrices for $\sigma(\pi^+\pi^-\gamma)$, $\sigma(\pi\pi)$, $|F_\pi(s)|^2$, the detector matrix, and the $\pi^+\pi^-\gamma$ observed spectrum are available from the corresponding authors.